Light Dark Matter Search with a High-Resolution Athermal Phonon Detector Operated Above Ground

I. Alkhatib,[1] D.W.P. Amaral,[2] T. Aralis,[3] T. Aramaki,[4] I.J. Arnquist,[5] I. Ataee Langroudy,[6] E. Azadbakht,[6] S. Banik,[7] D. Barker,[8] C. Bathurst,[9] D.A. Bauer,[10] L.V.S. Bezerra,[11,12] R. Bhattacharyya,[6] T. Binder,[13] M.A. Bowles,[14] P.L. Brink,[4] R. Bunker,[5] B. Cabrera,[15] R. Calkins,[16] R.A. Cameron,[4] C. Cartaro,[4] D.G. Cerdeño,[2,17] Y.-Y. Chang,[3] M. Chaudhuri,[7] R. Chen,[18] N. Chott,[14] J. Cooley,[16] H. Coombes,[9] J. Corbett,[19] P. Cushman,[8] F. De Brienne,[20] M. L. di Vacri,[5] M.D. Diamond,[1] E. Fascione,[19,12] E. Figueroa-Feliciano,[18] C.W. Fink,[21] K. Fouts,[4] M. Fritts,[8] G. Gerbier,[19] R. Germond,[19,12] M. Ghaith,[19] S.R. Golwala,[3] H.R. Harris,[22,6] N. Herbert,[6] B.A. Hines,[23] M.I. Hollister,[10] Z. Hong,[18] E.W. Hoppe,[5] L. Hsu,[10] M.E. Huber,[23,24] V. Iyer,[7] D. Jardin,[16] A. Jastram,[6] V.K.S. Kashyap,[7] M.H. Kelsey,[6] A. Kubik,[6] N.A. Kurinsky,[10] R.E. Lawrence,[6] A. Li,[11,12] B. Loer,[5] E. Lopez Asamar,[2] P. Lukens,[10] D. MacDonell,[11,12] D.B. MacFarlane,[4] R. Mahapatra,[6] V. Mandic,[8] N. Mast,[8] A.J. Mayer,[12] H. Meyer zu Theenhausen,[25] .M. Michaud,[20] E. Michielin,[11,12] N. Mirabolfathi,[6] B. Mohanty,[7] J.D. Morales Mendoza,[6] S. Nagorny,[19] J. Nelson,[8] H. Neog,[6] V. Novati,[5] J.L. Orrell,[5] S.M. Oser,[11,12] W.A. Page,[21] P. Pakarha,[19] R. Partridge,[4] R. Podviianiuk,[13] F. Ponce,[15] S. Poudel,[13] M. Pyle,[21] W. Rau,[12] E. Reid,[2] R. Ren,[18] T. Reynolds,[9] A. Roberts,[23] A.E. Robinson,[20] T. Saab,[9] B. Sadoulet,[21,26] J. Sander,[13] A. Sattari,[1] R.W. Schnee,[14] S. Scorza,[27] B. Serfass,[21] D.J. Sincavage,[8] C. Stanford,[15] J. Street,[14] D. Toback,[6] R. Underwood,[19,12] S. Verma,[6] A.N. Villano,[23] B. von Krosigk,[25] S.L. Watkins,[21,*] L. Wills,[20] J.S. Wilson,[6] M.J. Wilson,[1,25] J. Winchell,[6] D.H. Wright,[4] S. Yellin,[15] B.A. Young,[28] T.C. Yu,[4] E. Zhang,[1] H.G. Zhang,[8] X. Zhao,[6] and L. Zheng[6]

(SuperCDMS Collaboration)

J. Camilleri,[21,†] Yu.G. Kolomensky,[21,26] and S. Zuber[21]

[1] *Department of Physics, University of Toronto, Toronto, ON M5S 1A7, Canada*
[2] *Department of Physics, Durham University, Durham DH1 3LE, UK*
[3] *Division of Physics, Mathematics, & Astronomy, California Institute of Technology, Pasadena, CA 91125, USA*
[4] *SLAC National Accelerator Laboratory/Kavli Institute for Particle Astrophysics and Cosmology, Menlo Park, CA 94025, USA*
[5] *Pacific Northwest National Laboratory, Richland, WA 99352, USA*
[6] *Department of Physics and Astronomy, and the Mitchell Institute for Fundamental Physics and Astronomy, Texas A&M University, College Station, TX 77843, USA*
[7] *School of Physical Sciences, National Institute of Science Education and Research, HBNI, Jatni - 752050, India*
[8] *School of Physics & Astronomy, University of Minnesota, Minneapolis, MN 55455, USA*
[9] *Department of Physics, University of Florida, Gainesville, FL 32611, USA*
[10] *Fermi National Accelerator Laboratory, Batavia, IL 60510, USA*
[11] *Department of Physics & Astronomy, University of British Columbia, Vancouver, BC V6T 1Z1, Canada*
[12] *TRIUMF, Vancouver, BC V6T 2A3, Canada*
[13] *Department of Physics, University of South Dakota, Vermillion, SD 57069, USA*
[14] *Department of Physics, South Dakota School of Mines and Technology, Rapid City, SD 57701, USA*
[15] *Department of Physics, Stanford University, Stanford, CA 94305, USA*
[16] *Department of Physics, Southern Methodist University, Dallas, TX 75275, USA*
[17] *Instituto de Física Teórica UAM/CSIC, Universidad Autónoma de Madrid, 28049 Madrid, Spain*
[18] *Department of Physics & Astronomy, Northwestern University, Evanston, IL 60208-3112, USA*
[19] *Department of Physics, Queen's University, Kingston, ON K7L 3N6, Canada*
[20] *Département de Physique, Université de Montréal, Montréal, Qubec H3C 3J7, Canada*
[21] *Department of Physics, University of California, Berkeley, CA 94720, USA*
[22] *Department of Electrical and Computer Engineering, Texas A&M University, College Station, TX 77843, USA*
[23] *Department of Physics, University of Colorado Denver, Denver, CO 80217, USA*
[24] *Department of Electrical Engineering, University of Colorado Denver, Denver, CO 80217, USA*
[25] *Institut für Experimentalphysik, Universität Hamburg, 22761 Hamburg, Germany*
[26] *Lawrence Berkeley National Laboratory, Berkeley, CA 94720, USA*
[27] *SNOLAB, Creighton Mine #9, 1039 Regional Road 24, Sudbury, ON P3Y 1N2, Canada*
[28] *Department of Physics, Santa Clara University, Santa Clara, CA 95053, USA*

(Dated: July 29, 2020)

We present limits on spin-independent dark matter-nucleon interactions using a 10.6 g Si athermal phonon detector with a baseline energy resolution of $\sigma_E = 4.92 \pm 0.01$ eV. This exclusion analysis sets the most stringent dark matter-nucleon scattering cross-section limits for dark matter particle masses from 87 to 140 MeV/c^2, with a raw exposure of 9.9 g d acquired at an above-ground facility.

This work illustrates the scientific potential of detectors with athermal phonon sensors with eV-scale energy resolution for future dark matter searches.

Introduction.—Numerous observations have shown that the majority of the Universe is composed of non-luminous matter [1–3]. The weakly-interacting massive particle (WIMP) [4] has long been a favored candidate for this dark matter (DM). However, direct detection experiments have ruled out a significant portion of the most compelling WIMP parameter space [5–7], which has motivated both theoretical and experimental exploration of alternative DM models [8]. In particular, light dark matter (LDM) with a mass in the keV/c^2 to GeV/c^2 range which couples to Standard Model particles via a new force mediator provides a well-motivated alternative to the WIMP hypothesis [9–11]. While recent LDM searches have focused on DM-electron interactions [12–16], detectors with eV-scale energy thresholds can also be used to study LDM via DM-nucleon interactions.

We present results from a DM search with a new Cryogenic PhotoDetector (CPD) featuring an athermal phonon sensor with a baseline energy resolution of $\sigma_E = 4.92 \pm 0.01\,\mathrm{eV}$. Although this device was designed for active particle identification in rare event searches, such as for neutrinoless double-beta decay [17, 18] and DM, the excellent energy resolution motivated its use as a DM detector itself. As a combined effort of the SuperCDMS and CPD collaborations, a DM search was carried out with 9.9 g d of raw exposure from Sept. 9^{th} to 10^{th} 2018. The data were acquired at the SLAC National Accelerator Laboratory in a surface facility of $\sim 100\,\mathrm{m}$ in elevation. We discuss data acquisition techniques, device performance, and the results of an exclusion analysis for spin-independent DM-nucleon interactions.

Experimental setup.—The CPD substrate is a 1 mm thick Si wafer with a radius of 3.81 cm and a mass of 10.6 g. It is instrumented on one side with $\sim$1000 Quasiparticle-trap-assisted Electrothermal feedback Transition-edge sensors (QETs) [19, 20] distributed over the surface and connected in parallel to a single readout channel. The opposite side of the wafer is polished but not instrumented. The distributed channel results in minimal position dependence and fast collection of athermal phonons, which reduces inefficiency due to effects such as athermal phonon down-conversion [21, 22]. Operated at a nominal bath temperature of 8 mK, the eV-scale baseline energy resolution was achieved, thanks in part to the relatively low QET critical temperature of 41.5 mK.

A collimated ^{55}Fe source was placed facing the non-instrumented side. The electron capture decay provides Mn K_α and K_β X-ray lines at 5.9 and 6.5 keV, respectively, for *in situ* calibration [23]. A 38 μm layer of Al was placed in front of the collimator to attenuate the rate of these photons and provide an additional calibration line at 1.5 keV from Al fluorescence [24].

For the sensor readout, a direct-current superconducting quantum interference device (SQUID) array–based amplifier was used, similar in design to the one described in Ref. [25]. Due to project time constraints and large cosmogenic backgrounds, the DM search was limited to 22 hrs. Data were acquired over this period using a field-programmable gate array (FPGA) triggering algorithm based on the optimal filter (OF) formalism [26, 27]. Throughout the exposure, randomly triggered samples of the baseline noise were acquired ("in-run random triggers"), which allowed us to observe any changes in the noise over the course of the search and to calculate and monitor the baseline energy resolution.

The trigger threshold was set at $4.2\,\sigma$ above the baseline noise level, corresponding to 20.7 eV after calibration. The phonon-pulse template used for the FPGA triggering algorithm was a double-exponential pulse with a rise time of $\tau_r = 20\,\mu$s and a fall time of $\tau_f = 58\,\mu$s. The rise time was taken from the expected collection time of athermal phonons, and the fall time was taken from the thermal response time of the QET estimated from a measurement of the complex admittance [19]. Each of these time constants was confirmed by nonlinear least squares fits to nonsaturated pulses. Before starting the DM search, a separate, small subset of random triggers was collected. After removing data contaminated by effects such as elevated baselines and phonon pulses, the noise spectrum used by the FPGA algorithm was generated from these random triggers.

For overlapping triggered pulse traces, the triggering algorithm was set to save a trace centered on the pulse with the largest OF amplitude. We note that the FPGA triggering algorithm acted on a trace that was downsampled by a factor of 16, from the digitization rate of 625 kHz to 39 kHz. Additionally, the FPGA triggering algorithm considered only 26.2 ms of the total 52 ms long time trace saved for each triggered pulse trace ("event"). Because of these factors, the energy resolution of the FPGA triggering algorithm is not as good as can be achieved by reconstructing event energies using an offline OF, as described in the following sections.

While the FPGA-based OF was used to trigger the experiment in real time, we ultimately used an offline algorithm to reconstruct event energies, where we again used the OF formalism. For this offline OF, we were able to use a single noise spectrum computed from the in-run random triggers to represent the entire data set because there was negligible time variation of the noise over the course of the full exposure. Pulse amplitudes and start times were reconstructed using the same phonon-pulse template as in the FPGA triggering algorithm. Thus,

there are two different pulse amplitudes for each event—one from the FPGA triggering algorithm and one from the offline OF. In Fig. 1, we compare the different energy estimators for a representative event.

This detector was optimized for maximum energy sensitivity at low energies and does not have a large enough dynamic range to observe the calibration lines without nonlinear effects from saturation of the QETs. In particular, the spacing and amplitudes of the two ^{55}Fe lines demonstrate that the detector's energy response is nonlinear at high energies (cf. Fig. 2). The nonlinearity is minimal within our region-of-interest (ROI), which is below 300 eV. Above the ROI, the fall time of the pulses increases monotonically with energy, which can be explained by effects of local saturation. Localized events can saturate nearby QETs to above the superconducting transition, while QETs far from the event stay within the superconducting transition. Because this is a single-channel device, the saturated and unsaturated QETs are read out in parallel and thus effectively combine into a single phonon pulse with an increased fall time. As we do not have a complete understanding of these saturation effects, our choice of model would be arbitrary and have a nonnegligible effect on the reconstructed energy in our ROI. Thus, we made a conservative choice to calibrate the reconstructed energy linearly to the Al fluorescence line at 1.5 keV (see Fig. 2 inset). Because the ^{55}Fe K$_\alpha$ and K$_\beta$ lines show significant saturation, they are reconstructed to energies far from their expected values of 5.9 and 6.5 keV with this calibration. See the Supplemental Material for further discussion of this effect.

There is a systematic bias associated with this calibration that overestimates the baseline energy resolution, the trigger threshold, and the energies of events within the ROI. Shifting the threshold to higher energies significantly weakens limits on the DM interaction rate for low DM masses. For DM masses with characteristic recoil-energy scales that are far above threshold, the differential rates will be immune to this threshold effect. In this case, the systematic overestimate of the energies of events increases the differential rate for backgrounds that decrease with energy, such as the observed background in our ROI. Consequently, this calibration overall weakens our limits on the DM interaction rate such that our final results are conservative.

Data selection and efficiency.—We make our final event selection with a minimal number of selection criteria (cuts) to remove poorly reconstructed events without introducing energy dependence into the selection efficiency. This approach helps to reduce the complexity of the analysis and thus avoid introduction of systematic uncertainties. We apply two data-quality cuts: a prepulse baseline cut and a chi-square cut.

We define the event baseline as the average output in the prepulse section of each event, which is the first 25.6 ms of each trace. Large energy depositions have a

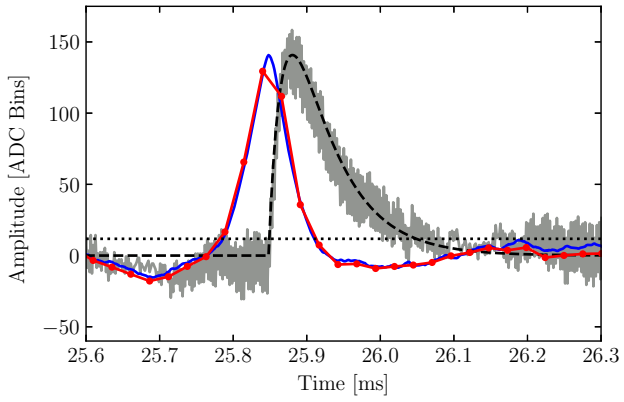

FIG. 1. A zoomed-in portion of an example event within the analysis ROI. The raw pulse (gray) is compared to the offline optimal filter result (blue), the pulse template scaled by the fit result (black dashed), the FPGA filter result (red with dots), and the FPGA trigger threshold (black dotted). The offline and FPGA optimal filters are highly correlated, but not exactly the same, with corresponding energy estimates for this event of 238 and 228 eV, respectively. The offset between the optimal filters and the raw pulse is an artifact of the filters, as they were set up to determine the time of the beginning of the pulse, as opposed to the maximum of the pulse.

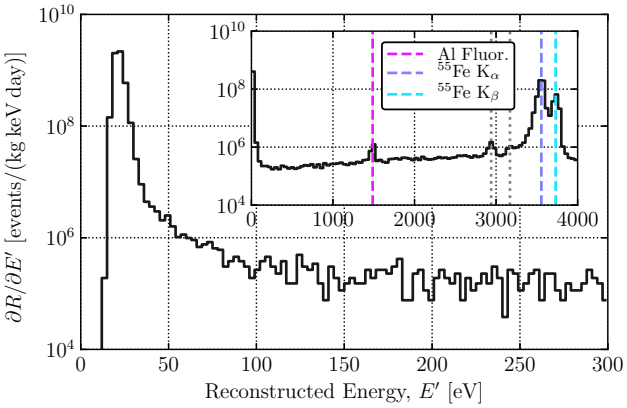

FIG. 2. Measured energy spectrum in the DM-search ROI for the full exposure after application of the quality cuts. The data have been normalized to events per kilogram per day per keV and have been corrected for the event-selection efficiency, but not the trigger efficiency. The inset shows the full spectrum up to 4 keV in reconstructed energy, noting the locations of the different spectral peaks. The known values of the marked lines are 1.5, 5.9, and 6.5 keV for the Al fluorescence, ^{55}Fe K$_\alpha$, and ^{55}Fe K$_\beta$ lines, respectively. The apparent increase in event rate with energy is an artifact of the distortion of the energy scale outside the ROI due to pulse-shape saturation. The two unlabeled lines (gray dotted) around 3 keV in reconstructed energy are the Si escape peaks [28].

long recovery time, which may manifest itself as a sloped baseline for subsequent events. Our trigger has reduced efficiency for any low-energy events occurring on such a baseline. We expected roughly 10% of the events to sit on the tail of a high energy event due to the nominal muon flux at the surface of $\sim 1\,\mathrm{muon/cm^2/min}$ [29]. The baseline cut is performed by binning the data across the search in 400 s long bins and removing from each bin the 10% of events that have the highest baseline. This energy-independent method removes 10% of the live time.

The chi-square cut is a general cut on our goodness-of-fit metric, for which we use the low-frequency chi-square χ^2_{LF} calculated from the offline OF fit [27]. This metric is similar to the χ^2 from the offline OF fit, but we truncate the integral at a cutoff frequency. This truncation allows us to remove sensitivity to superfluous degrees of freedom outside of our signal band from the chi-square, which reduces both the expected mean and the expected variance of the chi-square distribution. In this analysis, we used $f_{\mathrm{cutoff}} = 16\,\mathrm{kHz}$ because the rise and fall times of our expected pulse shape correspond to frequencies of 8.0 kHz and 2.7 kHz respectively. The pulse-shape variation within the DM-search ROI is minimal; this leads to a chi-square distribution that is largely independent of reconstructed event energy within this range. This in turn allows us to set an energy-independent cutoff value for χ^2_{LF}.

Our measured events cannot be used directly to measure the signal efficiency of the chi-square cut because they include some that are not representative of the expected DM signal, e.g. vibrationally-induced events, electronic glitches, pileup events, etc. Therefore, we created a pulse simulation by adding noise from the in-run random triggers to the pulse template, systematically scaling the latter over the range of energies corresponding to the DM-search ROI. We then process and analyze the simulated data in the same way as the DM-search data. In this case, the passage fraction of the chi-square cut, which has an energy-independent value of $98.53 \pm 0.01\%$, represents the cut's efficiency.

We do not apply any other cuts to the DM-search data. The total signal efficiency is thus 88.7% and is independent of energy. A variation of the cut values within reasonable bounds was found to have no significant impact on the experimental sensitivity.

Signal model.—In our DM signal model for spin-independent nuclear-recoil interactions [30], we use the standard astrophysical parameters for the dark matter velocity distribution [31–33]: a velocity of the Sun about the galactic center of $v_0 = 220\,\mathrm{km/s}$, a mean orbital velocity of the Earth of $v_E = 232\,\mathrm{km/s}$, a galactic escape velocity of $v_{\mathrm{esc}} = 544\,\mathrm{km/s}$, and a local DM density of $\rho_0 = 0.3\,\mathrm{GeV/cm^3}$. To take into account the trigger efficiency, we convolve the differential rate with the joint probability density function relating our two energy estimators, including the effects of the applied cuts. The signal model, which includes the estimated trigger efficiency, is given by

$$\frac{\partial R}{\partial E'}(E') = \int_0^\infty dE_T \int_0^\infty dE_0\, \Theta(E_T - \delta) \times \varepsilon(E', E_T, E_0) P(E', E_T|E_0) \frac{\partial R}{\partial E_0}(E_0), \quad (1)$$

where E_0 is the true recoil energy, E' is the recoil energy measured by the offline OF, E_T is the recoil energy measured by the FPGA triggering algorithm, δ is the trigger threshold set on the FPGA triggering algorithm, ε is the efficiency of the two quality cuts and two cuts that are applied to simulated data (as described in the following paragraphs), Θ represents the trigger threshold cut (a Heaviside function), and $P(E', E_T|E_0)$ is the probability to extract E' and E_T using the two energy reconstruction algorithms given the true recoil energy E_0. For the efficiency ε, we have generalized its form to be a function of energy, knowing that the baseline and chi-square cuts themselves are energy independent. The heat quenching factor (the ratio of heat signals produced by nuclear and electron recoils of the same energy that accounts for effects such as displacement damage) has been assumed to be unity for this work. Though measurements of the heat quenching factor have not been made for Si, similar work has been undertaken for Ge, where the heat quenching factor was shown to be very close to unity [34, 35].

The model in Eq. (1) was evaluated numerically, taking advantage of our pulse simulation. The pulse simulation includes a software simulation of the FPGA triggering algorithm, which had the same output as the hardware version when run on the DM-search data. With this simulation of the FPGA triggering algorithm, we can use the pulse simulation to determine $P(E', E_T|E_0)$ directly.

We also added two cuts to the simulated data only: a confidence ellipse cut and a trigger time cut. The confidence ellipse cut removed any events with an energy estimator value outside of the 99.7% confidence ellipse, which is defined by the covariance matrix of our two energy estimators for zero-energy events. This cut was implemented to exclude a scenario where a very small DM-induced nuclear recoil is estimated to have a significantly larger energy due to occurring in coincidence with a large experimental noise fluctuation. The trigger time cut removed events that were not within 29 μs—half of a fall time of a pulse—of the true event time, as determined by the energy-scaled pulse template. This cut ensured that the triggering algorithm was able to detect the signal added, as opposed to a large noise fluctuation elsewhere in the trace. These two cuts required knowledge of the true energy of the pulse—they cannot be applied to the data, but can be applied to the signal model—and helped to ensure that our signal modeling was conservative. In adding each of these cuts, we reduced our signal

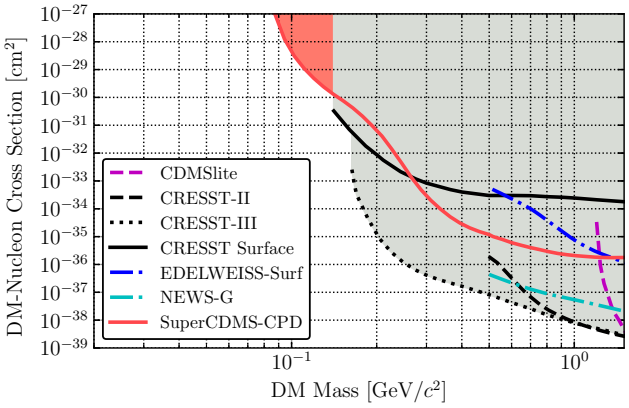

FIG. 3. The 90% C.L. limits on the spin-independent DM-nucleon cross section as a function of DM mass for this work (solid red line), compared to results from other experiments [38–43]. The previously ruled out parameter space from the latter are shown as the gray shaded region. The new parameter space ruled out from this search is shown as the red shaded region.

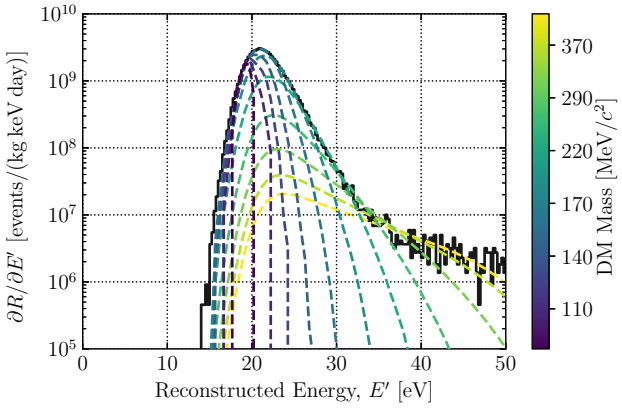

FIG. 4. The event spectrum for the DM search data below 50 eV in reconstructed energy. The data have been normalized to events per kilogram per day per keV and have been corrected for the signal efficiency of the data-quality cuts, but not the confidence-ellipse and trigger-time cuts. The colored dashed lines represent the calculated event rates for selected DM cross sections and masses from the 90% C.L. limit, where the optimum intervals in recoil energy are below 50 eV. Sensitivity to DM masses below 400 MeV/c^2 corresponds to recoil energies below 50 eV, with the lowest masses requiring energy sensitivity down to $\sim$20 eV.

efficiency estimate, which necessarily biased the results in the conservative direction.

Results.—The objective of this DM search was to set conservative 90% upper confidence limits on the spin-independent interaction of dark matter particles with masses below 1.5 GeV/c^2. We use the optimum interval (OI) method [36, 37] with unknown background, thus assuming that the full measured event rate could be due to a dark matter signal.

The results of the dark matter search are shown in Fig. 3, compared to other pertinent DM searches in the same parameter space [38–43]. For DM masses between 87 and 140 MeV/c^2, these results provide the most stringent limits for nuclear-recoil DM signals. For DM masses between 250 MeV/c^2 and 1.35 GeV/c^2, they are the most stringent limits achieved in an above-ground facility. With regard to strongly-interacting massive particles as DM candidates, we note that a cross-section limit associated with the facility's overburden [44, 45] has not been calculated for this search. It is expected to be greater than 10^{-27} cm^2, as the SLAC surface facility is likely to have an overburden similar to those in the CRESST and EDELWEISS above-ground DM searches [42, 46]. In Fig. 4, we show the data spectrum for reconstructed energies below 50 eV and DM signal curves for various DM masses, where the cross sections from the OI limit are used; the approximate location of the optimum interval is apparent for each dark matter mass.

In this search, we see an excess of events for recoil energies below about 150 eV, emerging above the roughly flat rate from Compton scattering of the gamma-ray background. We are actively investigating this excess of events by operating this detector in an environment with substantially reduced cosmogenic backgrounds.

Conclusion.—Using a detector with 4.92 ± 0.01 eV baseline energy resolution operated in an above-ground facility with an exposure of 9.9 g d, we exclude new parameter space for spin-independent interactions of DM with nucleons for light dark matter masses from 87 to 140 MeV/c^2. These results also set the most stringent limits for above-ground nuclear-recoil signals from dark matter for masses between 250 MeV/c^2 and 1.35 GeV/c^2. This was achieved using a single readout channel composed of QETs distributed on a Si substrate, with a recoil energy threshold set at 20.7 eV.

The results of this work were accomplished despite the high background rates in our surface facility because of the excellent baseline energy resolution of the detector. We plan to operate this detector in an underground laboratory, where we expect to have a significantly lower Compton scattering background rate. This will allow further study of the excess events observed in the ROI, hopefully providing insight into the origin of the event rate that is limiting the results reported here.

These results also demonstrate the potential of athermal phonon sensors with eV-scale baseline energy resolution for future dark matter searches via DM-nucleon interactions. Because this detector has a large surface area relative to its small volume, it is not optimal for a DM search. The baseline energy resolution of such devices scales with the number of QETs, which itself is proportional to the instrumented area (assuming the same QET design used by the CPD) [47, 48]. Thus, a decrease

in the instrumented area, with an increase in volume, should lead to improvements in baseline energy resolution. Future work is planned to design detectors of volume $\sim 1\,\mathrm{cm}^3$, for which it is reasonable to expect roughly an order of magnitude improvement in baseline energy resolution through these geometric considerations alone. With improved baseline energy resolution comes a lower energy threshold, allowing a search for spin-independent DM-nucleon interactions for even lower DM masses.

Acknowledgments.—Funding and support were received from the National Science Foundation, the U.S. Department of Energy (DOE), Fermilab URA Visiting Scholar Grant No. 15-S-33, NSERC Canada, the Canada First Excellence Research Fund, the Arthur B. McDonald Institute (Canada), Michael M. Garland, the Department of Atomic Energy Government of India (DAE), and the Deutsche Forschungsgemeinschaft (DFG, German Research Foundation)Project No. 420484612 and under Germanys Excellence Strategy - EXC 2121 "Quantum Universe" 390833306. Fermilab, PNNL, SLAC, and LBNL are operated under contracts DE-AC02-07CH11359, DE-AC05-76RL01830, DE-AC02-76SF00515, and DE-AC02-05CH11231, respectively, with the U.S. Department of Energy.

* samwatkins@berkeley.edu
† Now at Department of Physics, Virginia Tech, Blacksburg, VA 24061, USA

[1] M. Tanabashi *et al.* (Particle Data Group), Review of Particle Physics, Phys. Rev. D **98**, 030001 (2018).
[2] P. A. R. Ade *et al.* (Planck Collaboration), Planck 2015 results - XIII. Cosmological parameters, Astron. Astrophys. **594**, A13 (2016).
[3] D. Clowe, M. Bradač, A. H. Gonzalez, M. Markevitch, S. W. Randall, C. Jones, and D. Zaritsky, A Direct Empirical Proof of the Existence of Dark Matter, Astrophys. J. **648**, L109 (2006).
[4] G. Steigman and M. S. Turner, Cosmological constraints on the properties of weakly interacting massive particles, Nucl. Phys. B **253**, 375 (1985).
[5] E. Aprile *et al.* (XENON Collaboration), Dark Matter Search Results from a One Ton-Year Exposure of XENON1T, Phys. Rev. Lett. **121**, 111302 (2018).
[6] D. S. Akerib *et al.* (LUX Collaboration), Results from a Search for Dark Matter in the Complete LUX Exposure, Phys. Rev. Lett. **118**, 021303 (2017).
[7] X. Cui *et al.* (PandaX-II Collaboration), Dark Matter Results from 54-Ton-Day Exposure of PandaX-II Experiment, Phys. Rev. Lett. **119**, 181302 (2017).
[8] M. Battaglieri *et al.*, US Cosmic Visions: New Ideas in Dark Matter 2017: Community Report, arXiv:1707.04591.
[9] R. Essig, J. Mardon, and T. Volansky, Direct detection of sub-GeV dark matter, Phys. Rev. D **85**, 076007 (2012).
[10] R. Essig *et al.*, Dark Sectors and New, Light, Weakly-Coupled Particles, arXiv:1311.0029.
[11] J. Alexander *et al.*, Dark Sectors 2016 Workshop: Community Report, arXiv:1608.08632.
[12] R. Agnese *et al.* (SuperCDMS Collaboration), First Dark Matter Constraints from a SuperCDMS Single-Charge Sensitive Detector, Phys. Rev. Lett. **121**, 051301 (2018).
[13] O. Abramoff *et al.* (SENSEI Collaboration), SENSEI: Direct-Detection Constraints on Sub-GeV Dark Matter from a Shallow Underground Run Using a Prototype Skipper CCD, Phys. Rev. Lett. **122**, 161801 (2019).
[14] A. Aguilar-Arevalo *et al.* (DAMIC Collaboration), Constraints on Light Dark Matter Particles Interacting with Electrons from DAMIC at SNOLAB, Phys. Rev. Lett. **123**, 181802 (2019).
[15] R. Essig, A. Manalaysay, J. Mardon, P. Sorensen, and T. Volansky, First Direct Detection Limits on Sub-GeV Dark Matter from XENON10, Phys. Rev. Lett. **109**, 021301 (2012).
[16] E. Aprile *et al.* (XENON Collaboration), Light Dark Matter Search with Ionization Signals in XENON1T, Phys. Rev. Lett. **123**, 251801 (2019).
[17] T. Tabarelli de Fatis, Cerenkov emission as a positive tag of double beta decays in bolometric experiments, Eur. Phys. J. C. **65**, 359 (2010).
[18] W. R. Armstrong *et al.* (CUPID Collaboration), CUPID pre-CDR, arXiv:1907.09376.
[19] K. D. Irwin and G. C. Hilton, Transition-Edge Sensors, in *Cryogenic Particle Detection*, edited by C. Enss (Springer Berlin Heidelberg, Berlin, Heidelberg, 2005) pp. 63–150.
[20] K. D. Irwin, S. W. Nam, B. Cabrera, B. Chugg, and B. A. Young, A quasiparticletrapassisted transitionedge sensor for phononmediated particle detection, Rev. Sci. Instrum. **66**, 5322 (1995).
[21] A. G. Kozorezov, A. F. Volkov, J. K. Wigmore, A. Peacock, A. Poelaert, and R. den Hartog, Quasiparticle-phonon downconversion in nonequilibrium superconductors, Phys. Rev. B **61**, 11807 (2000).
[22] W. Knaak, T. Hauß, M. Kummrow, and M. Meißner, in *Phonon Scattering in Condensed Matter V*, edited by A. C. Anderson and J. P. Wolfe (Springer Berlin Heidelberg, Berlin, Heidelberg, 1986) pp. 174–176.
[23] G. Hölzer, M. Fritsch, M. Deutsch, J. Härtwig, and E. Förster, $K\alpha_{1,2}$ and $K\beta_{1,3}$ x-ray emission lines of the $3d$ transition metals, Phys. Rev. A **56**, 4554 (1997).
[24] J. Schweppe, R. D. Deslattes, T. Mooney, and C. J. Powell, Accurate measurement of Mg and Al $K\alpha_{1,2}$ X-ray energy profiles, J. Electron Spectrosc. **67**, 463 (1994).
[25] S. Hansen, F. DeJongh, J. Hall, B. A. Hines, M. E. Huber, T. Kiper, V. Mandic, W. Rau, T. Saab, D. Seitz, *et al.*, in *IEEE Nuclear Science Symposium Medical Imaging Conference* (Knoxville, TN, 2010) pp. 1392–1395.
[26] L. A. Zadeh and J. R. Ragazzini, Optimum Filters for the Detection of Signals in Noise, Proc. IRE **40**, 1223 (1952).
[27] S. R. Golwala, *Exclusion limits on the WIMP nucleon elastic scattering cross-section from the Cryogenic Dark Matter Search*, Ph.D. thesis, University of California, Berkeley (2000).
[28] S. J. B. Reed and N. G. Ware, Escape peaks and internal fluorescence in X-ray spectra recorded with lithium drifted silicon detectors, J. Phys. E Sci. Instrum. **5**, 582 (1972).
[29] M. P. De Pascale, A. Morselli, P. Picozza, R. L. Golden, C. Grimani, B. L. Kimbell, S. A. Stephens, S. J. Stochaj, W. R. Webber, G. Basini, *et al.*, Absolute spectrum and

charge ratio of cosmic ray muons in the energy region from 0.2 GeV to 100 GeV at 600 m above sea level, J. Geophys. Res. **98**, 3501 (1993).
[30] J. D. Lewin and P. F. Smith, Review of mathematics, numerical factors, and corrections for dark matter experiments based on elastic nuclear recoil, Astropart. Phys. **6**, 87 (1996).
[31] F. J. Kerr and D. Lynden-Bell, Review of galactic constants, Mon. Not. R. Astron. Soc. **221**, 1023 (1986).
[32] M. C. Smith, G. R. Ruchti, A. Helmi, R. F. G. Wyse, J. P. Fulbright, K. C. Freeman, J. F. Navarro, G. M. Seabroke, M. Steinmetz, M. Williams, *et al.*, The RAVE survey: constraining the local Galactic escape speed, Mon. Not. R. Astron. Soc. **379**, 755 (2007).
[33] R. Schnrich, J. Binney, and W. Dehnen, Local kinematics and the local standard of rest, Mon. Not. R. Astron. Soc. **403**, 1829 (2010).
[34] A. Benoit *et al.* (EDELWEISS Collaboration), Measurement of the response of heat-and-ionization germanium detectors to nuclear recoils, Nucl. Instrum. Methods Phys. Res. A **577**, 558 (2007).
[35] R. Agnese *et al.* (SuperCDMS Collaboration), Energy loss due to defect formation from ^{206}Pb recoils in SuperCDMS germanium detectors, Appl. Phys. Lett. **113**, 092101 (2018).
[36] S. Yellin, Finding an upper limit in the presence of an unknown background, Phys. Rev. D **66**, 032005 (2002).
[37] S. Yellin, Extending the optimum interval method, arXiv:0709.2701.
[38] R. Agnese *et al.* (SuperCDMS Collaboration), Low-mass dark matter search with CDMSlite, Phys. Rev. D **97**, 022002 (2018).
[39] G. Angloher *et al.* (CRESST Collaboration), Results on light dark matter particles with a low-threshold CRESST-II detector, Eur. Phys. J. C **76**, 25 (2016).
[40] A. H. Abdelhameed *et al.* (CRESST Collaboration), First results from the CRESST-III low-mass dark matter program, Phys. Rev. D **100**, 102002 (2019).
[41] G. Angloher *et al.* (CRESST Collaboration), Results on MeV-scale dark matter from a gram-scale cryogenic calorimeter operated above ground, Eur. Phys. J. C **77**, 637 (2017).
[42] E. Armengaud *et al.* (EDELWEISS Collaboration), Searching for low-mass dark matter particles with a massive Ge bolometer operated above ground, Phys. Rev. D **99**, 082003 (2019).
[43] Q. Arnaud *et al.* (NEWS-G Collaboration), First results from the NEWS-G direct dark matter search experiment at the LSM, Astropart. Phys. **97**, 54 (2018).
[44] G. D. Starkman, A. Gould, R. Esmailzadeh, and S. Dimopoulos, Opening the window on strongly interacting dark matter, Phys. Rev. D **41**, 3594 (1990).
[45] G. Zaharijas and G. R. Farrar, Window in the dark matter exclusion limits, Phys. Rev. D **72**, 083502 (2005).
[46] T. Emken and C. Kouvaris, How blind are underground and surface detectors to strongly interacting dark matter?, Phys. Rev. D **97**, 115047 (2018).
[47] Y. Hochberg, M. Pyle, Y. Zhao, and K. M. Zurek, Detecting superlight dark matter with Fermi-degenerate materials, J. High Energ. Phys. **2016**, 57 (2016).
[48] S. Knapen, T. Lin, M. Pyle, and K. M. Zurek, Detection of light dark matter with optical phonons in polar materials, Phys. Lett. B **785**, 386 (2018).

Light Dark Matter Search with a High-Resolution Athermal Phonon Detector Operated Above Ground: Supplemental Material

I. Alkhatib,[1] D.W.P. Amaral,[2] T. Aralis,[3] T. Aramaki,[4] I.J. Arnquist,[5] I. Ataee Langroudy,[6] E. Azadbakht,[6] S. Banik,[7] D. Barker,[8] C. Bathurst,[9] D.A. Bauer,[10] L.V.S. Bezerra,[11,12] R. Bhattacharyya,[6] T. Binder,[13] M.A. Bowles,[14] P.L. Brink,[4] R. Bunker,[5] B. Cabrera,[15] R. Calkins,[16] R.A. Cameron,[4] C. Cartaro,[4] D.G. Cerdeño,[2,17] Y.-Y. Chang,[3] M. Chaudhuri,[7] R. Chen,[18] N. Chott,[14] J. Cooley,[16] H. Coombes,[9] J. Corbett,[19] P. Cushman,[8] F. De Brienne,[20] M. L. di Vacri,[5] M.D. Diamond,[1] E. Fascione,[19,12] E. Figueroa-Feliciano,[18] C.W. Fink,[21] K. Fouts,[4] M. Fritts,[8] G. Gerbier,[19] R. Germond,[19,12] M. Ghaith,[19] S.R. Golwala,[3] H.R. Harris,[22,6] N. Herbert,[6] B.A. Hines,[23] M.I. Hollister,[10] Z. Hong,[18] E.W. Hoppe,[5] L. Hsu,[10] M.E. Huber,[23,24] V. Iyer,[7] D. Jardin,[16] A. Jastram,[6] V.K.S. Kashyap,[7] M.H. Kelsey,[6] A. Kubik,[6] N.A. Kurinsky,[10] R.E. Lawrence,[6] A. Li,[11,12] B. Loer,[5] E. Lopez Asamar,[2] P. Lukens,[10] D. MacDonell,[11,12] D.B. MacFarlane,[4] R. Mahapatra,[6] V. Mandic,[8] N. Mast,[8] A.J. Mayer,[12] H. Meyer zu Theenhausen,[25] .M. Michaud,[20] E. Michielin,[11,12] N. Mirabolfathi,[6] B. Mohanty,[7] J.D. Morales Mendoza,[6] S. Nagorny,[19] J. Nelson,[8] H. Neog,[6] V. Novati,[5] J.L. Orrell,[5] S.M. Oser,[11,12] W.A. Page,[21] P. Pakarha,[19] R. Partridge,[4] R. Podviianiuk,[13] F. Ponce,[15] S. Poudel,[13] M. Pyle,[21] W. Rau,[12] E. Reid,[2] R. Ren,[18] T. Reynolds,[9] A. Roberts,[23] A.E. Robinson,[20] T. Saab,[9] B. Sadoulet,[21,26] J. Sander,[13] A. Sattari,[1] R.W. Schnee,[14] S. Scorza,[27] B. Serfass,[21] D.J. Sincavage,[8] C. Stanford,[15] J. Street,[14] D. Toback,[6] R. Underwood,[19,12] S. Verma,[6] A.N. Villano,[23] B. von Krosigk,[25] S.L. Watkins,[21,*] L. Wills,[20] J.S. Wilson,[6] M.J. Wilson,[1,25] J. Winchell,[6] D.H. Wright,[4] S. Yellin,[15] B.A. Young,[28] T.C. Yu,[4] E. Zhang,[1] H.G. Zhang,[8] X. Zhao,[6] and L. Zheng[6]

(SuperCDMS Collaboration)

J. Camilleri,[21,†] Yu.G. Kolomensky,[21,26] and S. Zuber[21]

[1] *Department of Physics, University of Toronto, Toronto, ON M5S 1A7, Canada*
[2] *Department of Physics, Durham University, Durham DH1 3LE, UK*
[3] *Division of Physics, Mathematics, & Astronomy, California Institute of Technology, Pasadena, CA 91125, USA*
[4] *SLAC National Accelerator Laboratory/Kavli Institute for Particle Astrophysics and Cosmology, Menlo Park, CA 94025, USA*
[5] *Pacific Northwest National Laboratory, Richland, WA 99352, USA*
[6] *Department of Physics and Astronomy, and the Mitchell Institute for Fundamental Physics and Astronomy, Texas A&M University, College Station, TX 77843, USA*
[7] *School of Physical Sciences, National Institute of Science Education and Research, HBNI, Jatni - 752050, India*
[8] *School of Physics & Astronomy, University of Minnesota, Minneapolis, MN 55455, USA*
[9] *Department of Physics, University of Florida, Gainesville, FL 32611, USA*
[10] *Fermi National Accelerator Laboratory, Batavia, IL 60510, USA*
[11] *Department of Physics & Astronomy, University of British Columbia, Vancouver, BC V6T 1Z1, Canada*
[12] *TRIUMF, Vancouver, BC V6T 2A3, Canada*
[13] *Department of Physics, University of South Dakota, Vermillion, SD 57069, USA*
[14] *Department of Physics, South Dakota School of Mines and Technology, Rapid City, SD 57701, USA*
[15] *Department of Physics, Stanford University, Stanford, CA 94305, USA*
[16] *Department of Physics, Southern Methodist University, Dallas, TX 75275, USA*
[17] *Instituto de Física Teórica UAM/CSIC, Universidad Autónoma de Madrid, 28049 Madrid, Spain*
[18] *Department of Physics & Astronomy, Northwestern University, Evanston, IL 60208-3112, USA*
[19] *Department of Physics, Queen's University, Kingston, ON K7L 3N6, Canada*
[20] *Département de Physique, Université de Montréal, Montréal, Qubec H3C 3J7, Canada*
[21] *Department of Physics, University of California, Berkeley, CA 94720, USA*
[22] *Department of Electrical and Computer Engineering, Texas A&M University, College Station, TX 77843, USA*
[23] *Department of Physics, University of Colorado Denver, Denver, CO 80217, USA*
[24] *Department of Electrical Engineering, University of Colorado Denver, Denver, CO 80217, USA*
[25] *Institut für Experimentalphysik, Universität Hamburg, 22761 Hamburg, Germany*
[26] *Lawrence Berkeley National Laboratory, Berkeley, CA 94720, USA*
[27] *SNOLAB, Creighton Mine #9, 1039 Regional Road 24, Sudbury, ON P3Y 1N2, Canada*
[28] *Department of Physics, Santa Clara University, Santa Clara, CA 95053, USA*

(Dated: July 29, 2020)

Energy calibration saturation.—In the main text, we showed the spectrum of our events in reconstructed energy in the inset of Fig. 2, which exhibited noticeable saturation at high energies. The calibration in the dark

matter search was done to ensure that any bias introduced was in the conservative direction, as there was nonnegligible systematic error in how we modeled the saturation. In this supplemental material, we will briefly outline the calculation of an alternative energy metric that is much less susceptible to saturation effects and compare the result to the spectrum shown in the main text.

Due to saturation effects, event pulse shapes are seen to have monotonically increasing fall times with energy deposited. For energy estimators such as the optimal filter [1, 2] that assume a constant pulse shape, this effect leads to a sizable underestimation of the true event energy for large energy depositions. Energy estimators that use only DC pulse information are insensitive to such pulse-shape effects, but are also fundamentally less sensitive, since they do not use higher frequency information. The most natural DC estimator is the absolute calibration of the energy deposited in the transition-edge sensor (TES), which is calculated via

$$E_{\rm abs} = \int_0^\infty \left[(V - 2I_0R_\ell)\,\Delta I(t) - \Delta I(t)^2 R_\ell\right] dt, \quad (1)$$

where $\Delta I(t)$ is the baseline-subtracted pulse in current, I_0 is the quiescent current through the TES, R_ℓ is the load resistance, and V is the bias voltage of the circuit [3]. The second order term in $\Delta I(t)$ serves to reduce some of the saturation effects in the data at higher energies, as opposed to the simple integral.

This DC absolute energy estimator still displays $\sim$22% of saturation at the ^{55}K$_\alpha$ line. Physically, this is due to the fact that the thermal conductance between the TES and the thermal bath increases with TES temperature. This can be empirically corrected by fitting the calibration peaks to the following functional form:

$$E_{\rm abs} = a\left[1 - \exp\left(-\frac{E_{\rm true}}{b}\right)\right]. \quad (2)$$

The functional form in Eq. (2) was chosen because it has an intercept at zero, approaches an asymptotic value at high energies, and has only two fit parameters. Though such constraints on the saturation functional form are necessary, they are not sufficient. Thus, use of this saturation calibrated absorption energy produces difficult-to-quantify systematic error. By choosing the simplest, most conservative energy estimator, we removed this systematic error at the expense of decreased dark matter sensitivity.

In Fig. 1, we show a comparison of the spectrum using the reconstructed energy with a spectrum using the estimated true energy via the saturation-corrected absorbed energy. The corresponding calibration peaks in each energy estimator can be seen via the vertical lines. We see that the aluminum fluorescence line is at the same energy for both energy estimators. It is visually apparent that

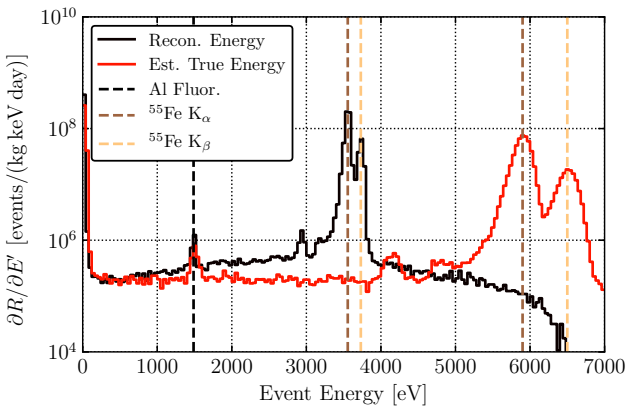

FIG. 1. A comparison of the spectrum from the reconstructed energy and the estimated true energy. The calibration lines denoted are the aluminum line at 1.5 keV [4], the ^{55}Fe K$_\alpha$ line at 5.9 keV, and the ^{55}Fe K$_\beta$ line at 6.5 keV [5]. The comparison of the two spectra shows the nonlinearity of the detector with energy.

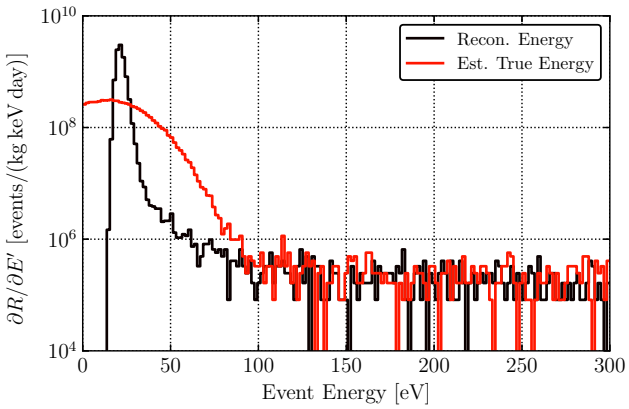

FIG. 2. A comparison of the spectrum from the reconstructed energy and the estimated true energy within the ROI of the DM search.

the conservative calibration used in the DM search has increased the measured differential rate, where this effect is considerable at high energies. We also see that the spectra converge in differential rate as we approach the region-of-interest (ROI) of the dark matter search (see Fig. 2), which is below 300 eV.

While the alternative energy metric has substantially less nonlinear behavior, the baseline energy resolution would be on the order of 20 eV. As the ROI for the DM search corresponds to energies below 300 eV, with sensitivity to the lowest DM masses corresponding to energies below 50 eV, we would not be able to use this metric without a significant loss in experimental sensitivity. We also studied using the alternative energy metric to calibrate the reconstructed energy from the offline optimal filter. However, the saturation modeling gave rise

to a systematic error on the order of 5–10% in reconstructed energy, which motivated being conservative in our calibration. The distribution of the systematic error associated with this correction would not have been well-understood, which would have resulted in a banded limit that was not statistically well-motivated.

* samwatkins@berkeley.edu
† Now at Department of Physics, Virginia Tech, Blacksburg, VA 24061, USA

[1] L. A. Zadeh and J. R. Ragazzini, Optimum Filters for the Detection of Signals in Noise, Proc. IRE **40**, 1223 (1952).
[2] S. R. Golwala, *Exclusion limits on the WIMP nucleon elastic scattering cross-section from the Cryogenic Dark Matter Search*, Ph.D. thesis, University of California, Berkeley (2000).
[3] K. D. Irwin and G. C. Hilton, Transition-Edge Sensors, in *Cryogenic Particle Detection*, edited by C. Enss (Springer Berlin Heidelberg, Berlin, Heidelberg, 2005) pp. 63–150.
[4] J. Schweppe, R. D. Deslattes, T. Mooney, and C. J. Powell, Accurate measurement of Mg and Al K$\alpha_{1,2}$ X-ray energy profiles, J. Electron Spectrosc. **67**, 463 (1994).
[5] G. Hölzer, M. Fritsch, M. Deutsch, J. Härtwig, and E. Förster, $K\alpha_{1,2}$ and $K\beta_{1,3}$ x-ray emission lines of the 3d transition metals, Phys. Rev. A **56**, 4554 (1997).